JACS
JOURNAL OF THE AMERICAN CHEMICAL SOCIETY
Article
Cite This: J. Am. Chem. Soc. 2019, 141, 4613−4623
pubs.acs.org/JACS

Direct Identification of Active Surface Species for the Water−Gas Shift Reaction on a Gold−Ceria Catalyst

Xin-Pu Fu,[†] Li-Wen Guo,[†] Wei-Wei Wang,[†] Chao Ma,[§] Chun-Jiang Jia,*[,†] Ke Wu,[∥] Rui Si,*[,‡] Ling-Dong Sun,[∥] and Chun-Hua Yan*[,∥]

[†]Key Laboratory for Colloid and Interface Chemistry, Key Laboratory of Special Aggregated Materials, School of Chemistry and Chemical Engineering, Shandong University, Jinan 250100, China

[‡]Shanghai Synchrotron Radiation Facility, Shanghai Institute of Applied Physics, Chinese Academy of Sciences, Shanghai 201204, China

[§]College of Materials Science and Engineering, Hunan University, Changsha 410082, China

[∥]Beijing National Laboratory for Molecular Sciences, State Key Laboratory of Rare Earth Materials Chemistry and Applications, PKU-HKU Joint Laboratory in Rare Earth Materials and Bioinorganic Chemistry, Peking University, Beijing 100871, China

Supporting Information

ABSTRACT: The crucial role of the metal−oxide interface in the catalysts of the water−gas shift (WGS) reaction has been recognized, while the precise illustration of the intrinsic reaction at the interfacial site has scarcely been presented. Here, two kinds of gold−ceria catalysts with totally distinct gold species, <2 nm clusters and 3 to 4 nm particles, were synthesized as catalysts for the WGS reaction. We found that the gold cluster catalyst exhibited a superiority in reactivity compared to gold nanoparticles. With the aid of comprehensive in situ characterization techniques, the bridged −OH groups that formed on the surface oxygen vacancies of the ceria support are directly determined to be the sole active configuration among various surface hydroxyls in the gold−ceria catalysts. The isotopic tracing results further proved that the reaction between bridged surface −OH groups and CO molecules adsorbed on interfacial Au atoms contributes dominantly to the WGS reactivity. Thus, the abundant interfacial sites in gold clusters on the ceria surface induced superior reactivity compared to that of supported gold nanoparticles in catalyzing the WGS reaction. On the basis of direct and solid experimental evidence, we have obtained a very clear image of the surface reaction for the WGS reaction catalyzed by the gold−ceria catalyst.

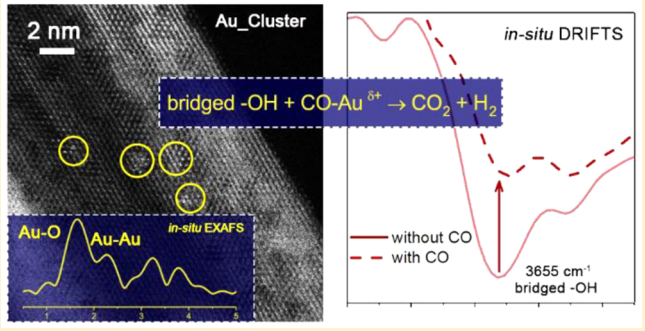

INTRODUCTION

The water−gas shift (WGS) reaction ($CO + H_2O \rightarrow H_2 + CO_2$) is crucial in the H_2 purification process for practical proton-exchange membrane (PEM) fuel cells and other industrial applications in which the residual CO harms the electrode and catalyst.[1−7] Gold supported on reducible metal oxides, such as ceria[2,3,7] and titanium,[6] has received considerable attention for its excellent WGS reaction activity at low temperatures (<300 °C). The importance of the metal−oxide interface has been recognized momentously for the WGS reaction.[3,6,8−13] However, because of the structural complexity of supported gold catalysts, understanding the actual surface reaction at metal−oxide interfaces is significant deepened.

On the basis of experimental and theoretical investigations on the inverse TiO_x/Au(111) model catalyst, Rodriguez et al. concluded that the metal−support interface was critical for water activation in producing active hydroxyls,[3] which was considered to be the rate-limiting step for the WGS reaction.[14] However, the exact role of dissociated −OH derived from water activation in the WGS reaction is still unclear. With respect to (Au,Pt)/CeO_2 powder catalysts, Flytzani-Stephanopoulos and co-workers elucidated that a refined M−OH_x interfacial structure could facilitate WGS reactivity and proved that −OH groups were directly involved in the surface reaction.[2,12] Also, the role of surface −OH groups in the WGS reaction were also discussed in some other catalyst systems, such as CeO_2,[15] Au/MgO,[16] and Cu.[17] These studies all implied the participation of −OH groups in the WGS surface reaction. However, limited by the complexity of a practical catalyst surface in which dry $[O]^2$ and multiple kinds of hydroxyl species (terminal, bridged, and three-coordinate −OH) were found,[18] there is still a lot of uncertainty and debate in revealing the precise role of surface hydroxyl groups.[16,17,19] In particularly, the authentic configuration and exact contribution of active −OH groups in catalyzing the WGS reaction has not yet been clearly determined.

Received: August 29, 2018
Published: February 26, 2019

DOI: 10.1021/jacs.8b09306
J. Am. Chem. Soc. 2019, 141, 4613−4623

Besides the limited understandings of the exact role of the surface hydroxyls, the active site for CO adsorption in the WGS reaction on catalysts is also unclear and under debate. Using Au/CeO_2 catalyst as an example, Flytzani-Stephanopoulos et al. concluded that oxidic Au acts as the active species in the low-temperature WGS reaction.[1,2,7] Kim et al.[20] and Behm et al.[21] concluded that reduced Au (Au^0) presents the active Au species. In fact, the status of gold is directly related to the positions (at the interfacial site or on the surface of gold particles) of gold atoms on the surface of the support. To precisely identify the real active gold site for CO adsorption in the WGS reaction, both the electronic structure and positions of the gold species must be considered. Therefore, comparable catalyst systems which contain distinct gold-support interfacial structures are significant in design and preparation.

In this work, two kinds of gold species (<2 nm disordered clusters (Au_Cluster) and 3 to 4 nm crystalline particles (Au_Particle)) were supported on the same ceria nanorods as catalysts for the WGS reaction. To reveal the intrinsic role of the metal−oxide interface in the WGS reaction, we performed in situ X-ray absorption fine structure (XAFS), in situ diffuse reflectance infrared Fourier transform spectroscopy (DRIFTS), and in situ Raman measurements on Au_Cluster and Au_Particle catalysts. Correlations between the WGS reactivity and in situ characterization results veritably reveal that the bridged surface −OH group in the gold−ceria catalyst is the sole active configuration that is favorable to reaction with the adsorbed active CO-$Au^{\delta+}$ ($0 < \delta < 1$) molecules, which results in superior WGS performance for Au_Cluster.

EXPERIMENTAL METHODS

Catalyst Preparation. *Preparation of Ceria Nanorods.* The ceria nanorods were synthesized according to the hydrothermal method.[22] $Ce(NO_3)_3{\cdot}6H_2O$ (4.5 mmol) was added to an aqueous NaOH (6 M, 60 mL) solution under vigorous stirring. After the precipitation process was completed (ca. 10 min), the stock solution was transferred to a Teflon bottle and then tightly sealed in a stainless-steel autoclave. The hydrothermal procedure was carried out in a temperature-controlled electric oven at 100 °C for 24 h. The precipitates were separated by centrifugation and then washed with distilled water four times and with ethanol once. The ceria products were obtained by drying the as-washed product in air at 70 °C overnight.

Preparation of the Au_Particle Catalyst. The Au_Particle sample was prepared by a colloidal deposition (CD) method,[23] with 2 mL of a 0.0125 mol/L $HAuCl_4$ solution and 0.675 mL of a 0.5 wt % poly(vinyl alcohol) (PVA, M_w = 10,000 from Aldrich, 80% hydrolyzed) added to 48 mL of ultrapure water (18.25 MΩ) at room temperature under vigorous stirring. After 10 min, the rapid injection of 1.30 mL of a fresh 0.1 mol/L $NaBH_4$ aqueous solution led to the formation of a wine-red solution. Then, 0.5 g of the ceria support was added to the above colloidal gold solution immediately. After stirring for 0.5 h, the sample was washed with ultrapure water several times in order to remove the dissolved impurities. The gold−ceria sample was obtained after drying (60 °C, in air, for 12 h) and further calcination at 400 °C for 4 h in air.

Preparation of the Au_Cluster Catalyst. The Au_Cluster catalysts were prepared by a deposition-precipitation method[7] and generated under the WGS reaction conditions. The ceria support (1 g) was dispersed in 50 mL of ultrapure water by vigorous stirring for about 10 min. Then, an ammonium carbonate solution (25 mL, 1 M) was added to keep the pH value at 9. $HAuCl_4{\cdot}3H_2O$ (25 mL, 2.32 mM) was added to the stock solution dropwise. After the sample was aged for 1 h, 70 °C water was used to wash it. After drying (75 °C, in air, for 12 h) and further calcination (400 °C, in air, for 4 h), the yellow gold−ceria sample was obtained.

Characterization of Catalysts. *Surface Area of Catalysts.* The nitrogen sorption measurements were made in a Builder SSA-4200 surface area analyzer at 77 K after a degassing process at 200 °C for 6 h under vacuum. The pore size distribution of each replica was calculated by applying the BJH method. The surface area of each replica was calculated by using the BET method.

X-ray Diffraction (XRD). The X-ray diffraction (XRD) pattern of spent catalysts was carried out on the X7B beamline (λ = 0.3196 Å) of the National Synchrotron Light Source (NSLS) at Brookhaven National Laboratory (BNL). Two-dimensional XRD patterns were collected with an image-plate detector (PerkinElmer), and the powder rings were integrated using the FIT2D code. The diffraction angles have been converted to the wavelength of Cu Kα1 (1.5406 Å) in all of the reported patterns.

Transmission Electron Microscopy (TEM). HRTEM and HAADF-STEM images were recorded on a JEOL ARM200F microscope equipped with a probe-forming spherical-aberration corrector. Owing to the high Z (58) of the Ce atoms, the contrast of Au (Z = 79) in HAADF images is not clear, particularly for the thick region. Here, to enhance the contrast difference between Au and Ce, we set the inner and outer angles of the HAADF detector to 90 and 370 mrad, respectively, and the convergence angle to ca. 30 mrad. The spherical aberration coefficient was set to 0.5 mm.

Inductively Coupled Plasma−Atomic Emission Spectroscopy (ICP−AES). For both catalysts, the ICP−AES measurements were carried out on an IRIS Intrepid II XSP instrument (Thermo Electron Corporation).

Temperature Program Reduction by Hydrogen (H_2-TPR). The reduction evolution profile of both catalysts was conducted on a Builder PCSA-1000 instrument equipped with a thermal conductivity detector (TCD) to detect H_2 consumption. The sieved catalysts (20−40 mesh, ca. 30 mg) were heated (5 °C/min) from room temperature to 300 °C in a 5% H_2/Ar_2 (30 mL/min) gas mixture. Before each measurement, the fresh sample was pretreated in pure O_2 at 300 °C for 30 min to outgas the physically adsorbed species on the surface of the catalyst. To get the real reduction behavior of Au_Cluster, the profile was collected for the second round without any reoxidation.

X-ray Absorption Fine Structure (XAFS). The ex situ XAFS measurements on the fresh samples were performed on the BL14W1 beamline of the Shanghai Synchrotron Radiation Facility (SSRF), operated at 3.5 GeV in "top-up" mode with a constant current of 220 mA. The XAFS spectra were collected in fluorescence mode with a 32-element solid-state detector (SSD). The in situ XAFS experiments were conducted at the X18B beamline of NSLS at BNL, operated at 2.8 GeV in "decay" mode with currents of 160−300 mA. The powder sample (~25 mg) was loaded into a Kapton tube (o.d. = 0.125 in.) which was attached to an in situ flow cell. All of the catalysts were in situ taken under similar pretreatment with a catalytic test in the reaction cell: kept at 300 °C in synthetic air (99.997%, 30 mL/min) for 0.5 h and followed under WGS reactions (1% CO/~3% H_2O in He, 20 mL/min) at 300 °C for 1 h. Two small resistance heating wires were installed above and below the tube, and the temperature was monitored with a 0.5 mm chromel−alumel thermocouple that was placed inside the tube near the sample. Each XAFS spectrum (ca. 15 min collection) was taken in fluorescence mode with a four-element Vortex Silicon Drift Detector (SDD). The energy was calibrated for each scan with the first inflection point of the Au L-III edge in Au metal foil. The X-ray absorption near-edge spectroscopy (XANES) and extended X-ray absorption fine structure (EXAFS) data have been analyzed using the Athena and Artemis programs. For the XANES part, the experimental absorption coefficients as a function of energy $\mu(E)$ were processed by background subtraction and normalization procedures, and reported as "normalized absorption" with E_0 = 11 919.0 eV for all of the gold−ceria samples. For the EXAFS part, the Fourier-transformed (FT) data in R space were analyzed by applying first-shell approximate and metallic Au models for Au−O and Au−Au contributions. The passive electron factors, S_0^2, were determined by fitting the experimental data on Au foils and fixing the coordination number (CN) of Au−Au to be 12 and then fixing CN for further analysis of the measured samples. The parameters describing the

DOI: 10.1021/jacs.8b09306
J. Am. Chem. Soc. 2019, 141, 4613−4623

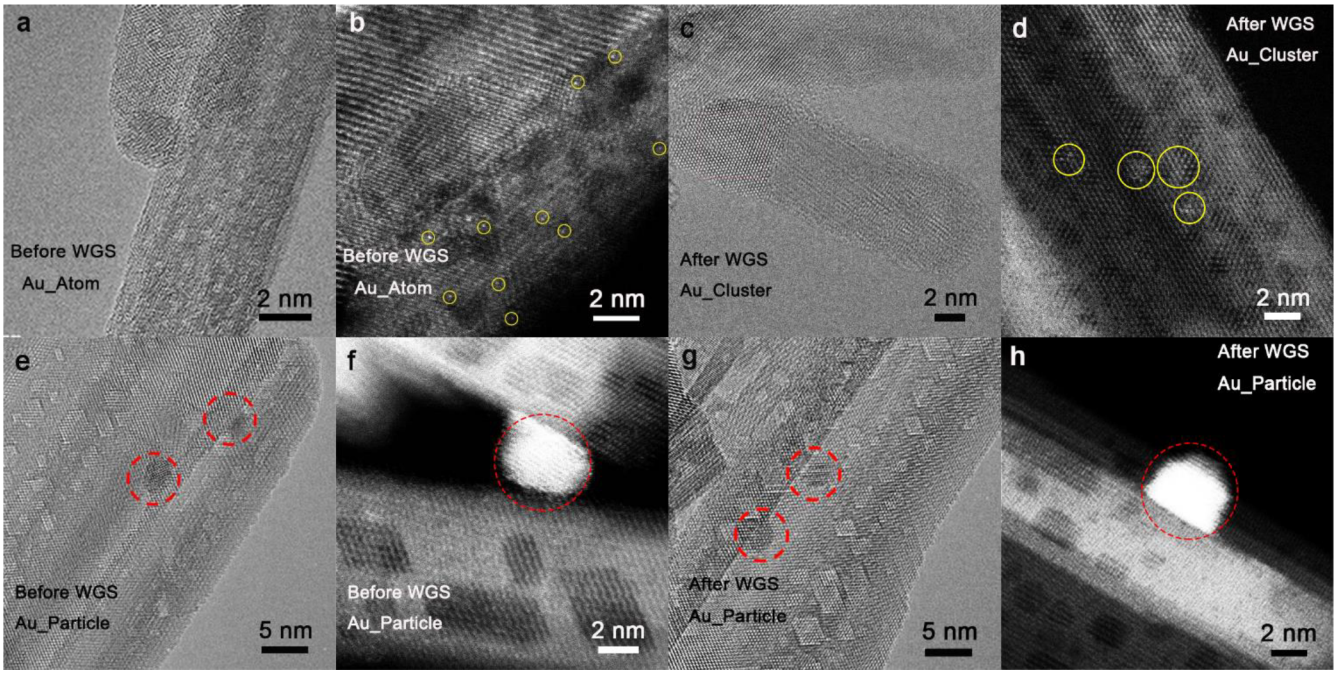

Figure 1. HRTEM image and aberration-corrected HAADF-STEM images of (a and b) the Au_Atom catalysts before WGS and (c and d) the Au_Cluster catalysts after the WGS test at 250 °C for 10 h, with gold atoms and clusters marked in yellow circles. (e and f) Au_Particle catalysts before the WGS reaction (after activation under a synthetic air feed at 300 °C) and (g and h) Au_Particle catalysts after the WGS test at 250 °C for 10 h, with gold particles marked in dashed red circles.

electronic properties (e.g., correction to the photoelectron energy origin, E_0) and local structural environment including the CN, bond distance (R), and Debye−Waller factor around the absorbing atoms were allowed to vary during the fitting process. The fitted ranges for k and R spaces were selected to be k = 3−11 Å^{-1} with R = 1−3 Å (k^3-weighted).

In Situ Diffuse Reflectance Infrared Fourier Transform Spectroscopy (DRIFTS). All of the in situ DRIFTS spectra were collected by using a Bruker Vertex 70 FTIR spectrometer equipped with a mercury cadmium telluride (MCT) detector. The DRIFTS reaction cell (Harrick) equipped with calcium fluoride windows has a heating cartridge that allowed samples to be heated controllably. To get an ultrabit dead volume during operation, the electro-control quick switching system was used to rapidly change the various gases. The intensities of IR bands were evaluated in Kubelka−Munk units, which were linearly proportional to the coverage of adsorbed surface species.[24] About 20 mg of all the catalysts were pretreated in situ in the reaction cell before the test in a manner similar to that used for the catalytic test: kept at 300 °C in synthetic air (99.997%, 30 mL/min) for 0.5 h, following under WGS reactions (2% CO/∼3% H_2O in He, 30 mL/min) at 300 °C for 1 h. Steady-state mode for all of the catalysts was used in the gas mixture (2% CO/∼3% H_2O in He, 30 mL/min) at 150 or 250 °C. For all of the in situ DRIFTS measurements with water injection, a certain number (∼3% H_2O in molar) of gaseous water molecules were carried into the reaction chamber by the mixed gas passing through the liquid water at room temperature, and the saturated vapor of water is present at ∼3 kPa. The CO adsorption mode under various temperatures was conducted in a 2% CO/He atmosphere, in which the CO gas (99.997%) was further predried through a liquid nitrogen trap. Typically, an acquisition time of 30 s with a resolution of 4 cm^{-1} was used for all spectrum collection. On one hand, to detect CO and CO_2 adsorption information, the background profiles were separately subtracted using a spectrum recorded in pure He (further dried through a cold well at 77 Kelvin) at the same temperature as above. On the other hand, for the surface information in the −OH region, the raw spectra were finally illustrated. For all of the tests, the prehydroxylation procedure was achieved by inducing ∼3% H_2O/He into the reaction chamber, followed by pure He purging (further predried through a cold well at 77 Kelvin) at 200 °C to remove residual molecular water on the surface.

In Situ Raman Test. All of the in situ Raman spectra were collected by using a LabRAM HR800 spectrometer (HORIBA JY) with laser excitation at 473 nm. The micro-Raman reaction cell (Xiamen TOPS) equipped with a quartz window has a heating module that allowed samples to be heated controllably. Similarly, for an ultrabit dead volume during operation, one six-way valve was used to rapidly switch the various gases. Before the test, about 30 mg of all of the catalysts were in situ pretreated similarly with a catalytic test in the reaction cell: held at 300 °C in synthetic air (99.997%, 30 mL/min) for 0.5 h, followed by WGS reactions (2% CO/∼3% H_2O in He, 30 mL/min) at 300 °C for 1 h. After outgassing by pure He gas, two kinds of measurements were conducted as follows.

First mode: For all catalysts (Au_Cluster, Au_Particle, and CeO_2 reference), three kinds of feeds (2% CO/He, ∼3% H_2O/He, and 2% CO/∼3% H_2O/He) with a flow rate of 30 mL/min were induced into the reaction chamber at 150 °C in turn. Second mode: Switch experiments for the Au_Cluster catalyst between 2% CO/∼3% H_2O/He (30 mL/min) and 5% H_2/∼3% H_2O/He (30 mL/min) were performed to further identify the role of surface oxygen vacancies. To obtain more precise information, all of the Raman spectra were obtained with a prolonged collection time of 15 min. For all of the in situ Raman measurements with water injection, a certain number (∼3% H_2O by mole) of the gaseous water molecules were carried into the reaction chamber by the mixed gas passing through the liquid water at room temperature such that the saturated vapor of water is present at ∼3 kPa.

Catalytic Tests and Kinetics Measurements. *Catalytic Performance.* The water−gas shift (WGS) reactivity of gold−ceria samples was measured in a fixed-bed reactor at atmospheric pressure. The reactor is a stainless-steel tube with an inner diameter of 8 mm, and the thermocouple is fixed on the catalyst bed inside. Sieved catalyst (20−40 mesh, 100 mg) was used in a gas mixture of 2% CO/12% H_2O/N_2 (99.997% purity), and the space velocity is 42 000 mL·h^{-1}·g_{cat}^{-1}. Prior to the measurement, the catalyst was pretreated in air (300 °C, 30 min) and then under WGS reactions (2% CO/12% H_2O in He, 30 mL/min) at 300 °C for 1 h. The stability tests were carried out at 250 °C for over 80 h. The unreacted water in the exhaust line

DOI: 10.1021/jacs.8b09306
J. Am. Chem. Soc. 2019, 141, 4613−4623

was condensed with an ice trap after the reactor tube. The outlet gas compositions of CO and CO_2 were measured with an infrared gas analyzer (Gasboard-3100, Wuhan Sifang Corp.).

Apparent Activation Energy (E_a) and Apparent Kinetic Orders. For both catalysts, the E_a was measured with the same reactor for catalytic performance above. Appropriate amounts of both Au_Cluster and Au_Particle catalysts diluted with SiO_2 (the corresponding height was less than 8 mm) were used in the kinetics experiments. The experiments were carried out by changing the temperature and the gas flow rate, with conversion not exceeding 15%. The product gas was measured with the infrared gas analyzer (Gasboard-3100, Wuhan Sifang Corp.). To determine the CO and H_2O reaction order, the concentration of CO was changed from 3 to 18%; the concentration of H_2O was changed from 4 to 20% during measurements, respectively.

Temperature Programed Surface Reaction (TPSR). For both catalysts, the activation steps were the same as for the catalytic tests above. After activation, samples were prehydroxylated with 30 mL/min ~3% H_2O/He for 5 min and then purged with pure He gas at 200 °C for another 30 min to purge adsorbed water molecules. A certain number (~3% H_2O by mole) of the gaseous water molecules were carried into the reaction chamber by the He flow passing through the liquid water at room temperature. For an ultrabit dead volume during operation, one six-way valve was used to rapidly switch the various gases, and the catalysts were not exposed to air after the activation step. To monitor the surface reaction with CO molecules, after activation, the gas was switched to 30 mL/min 2% CO/He for 20 min at 25 °C and then ramped to 600 °C at a heating rate of 5 °C/min. For the comparison test, after the prehydroxylation process described above, the Au_Cluster catalyst was then exposed to 30 mL/min pure He and finally ramped to 600 °C to observe the surface reaction without a CO feed. For the measurements of an isotopic tracer (H_2O^{18}) to probe the CO_2 origin during the α stage, the same as above, after prehydroxylation with ~3% H_2O^{18}/He and purging with pure He gas at 200 °C, the samples were exposed to 30 mL/min 2% CO/He and then ramped to 150 °C at a ramping rate of 5 °C/min.

RESULTS AND DISCUSSION

Structure and Catalytic Performance. The gold−ceria catalysts were first characterized by XRD and HRTEM. For the catalyst prepared by the deposition precipitation method, from the XRD patterns (Figure S1), fluorite cubic ceria was the major phase, and no discernible peak of gold was detected. The aberration-corrected HAADF-STEM images showed that isolated gold single atoms were anchored to the CeO_2 nanorod surface (Au_Atom, Figure 1a,b). However, these gold single atoms were unstable and easily transformed into gold clusters with diameters of <2 nm (Au_Cluster) under WGS reaction conditions, as shown in Figure 1c,d. Therefore, the gold cluster catalyst was obtained in situ during the WGS reaction with supported gold single atoms as precursors. As a contrast, gold nanoparticles with an average size of ≅3 to 4 nm (Au_Particle, Figure 1e,f)) supported on CeO_2 nanorods were prepared by the colloid deposition method. From the HAADF-STEM images, a negligible change could be detected for the as-formed gold nanoparticles after the WGS test (Figure 1g,h).

To get the electronic structure and coordination environment of the gold species in these gold−ceria catalysts, XAFS measurements were conducted. In situ XANES spectra in Figure 2a showed that the oxidation state of gold for Au_Particle was invariably maintained as Au^0. In contrast, for Au_Atom, the precursor of the Au_Cluster, in situ XANES spectra collected under pretreatment conditions revealed the fully oxidized state of gold (An^{n+}, $n > 1$) and coupling with a sole Au−O coordination in the first shell (R = 1.96 Å, CN = 3.3, Figure 2b). This was well in line with the structural feature of gold single atoms. Under WGS reaction conditions, gold single atoms transformed into gold clusters. Correspondingly, a slightly positive state of gold was detected for Au_Cluster from the in situ XANES spectra (Figure 2c), which was consistent with the XPS results (Figure S2). The in situ EXAFS spectra (Figure 2d), together with the corresponding fitting results (Table 1), revealed that the pure Au−Au contribution (R = 2.85 Å, CN = 11.5) was determined for Au_Particle. The peak splitting of Au−Au is due to Ramsauer−Townsend resonance at a single energy in the backscattering amplitude of Au. Au_Cluster catalyst showed a highly disordered structure and exhibited only about 1/5 EXAFS intensity of that for Au_Particle. Both Au−O shell (R = 2.02 Å, CN = 0.8) and Au−Au shells (R = 2.85 Å, CN = 0.9) were observed for Au_Cluster.

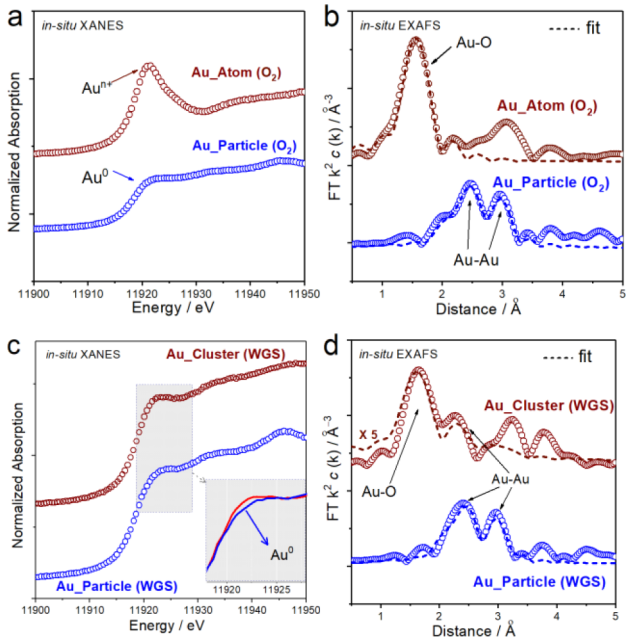

Figure 2. (a) In situ XANES spectra and (b) in situ EXAFS spectra collected under pretreatment at 300 °C in synthetic air for Au_Cluster and Au_Particle catalysts. (c) In situ XANES spectra; the shadowed illustrations are the enlarged area. (d) In situ EXAFS spectra of Au_Cluster and Au_Particle under WGS reaction conditions at 250 °C and the spectral intensity of Au_Cluster magnified at 5× for better comparison. Reaction condition for the in situ XAFS measurements: 1% CO/~3% H_2O/He, 20 mL/min, 250 °C, time on stream (TOS) = 1 h.

The catalytic properties of Au_Cluster and Au_Particle for the WGS reaction were evaluated. Compared to Au_Particle that had very low WGS activity, the Au_Cluster exhibited greatly enhanced reactivity especially at temperatures below 300 °C, which was shown in Figure 3a. Au_Particle exhibited very stable catalytic performance with a CO conversion of ca. 20% at 250 °C within the reaction time of ~80 h (Figure 3b). The HRTEM results of the spent catalysts showed that no obvious growth or agglomeration of gold nanoparticles was observed (Figure S3). For the Au_Cluster catalyst, a slight and gradual deactivation (from 83 to 51% in CO conversion) was found in the long term test (Figure 3b), which might be induced by the agglomeration of Au species (Figures S4 and S5) and blocking reaction sites by the accumulation of surface carbonaceous material.[19,20] To determine the intrinsic reason

DOI: 10.1021/jacs.8b09306
J. Am. Chem. Soc. 2019, 141, 4613−4623

Table 1. In Situ EXAFS Fitting Results of Gold−Ceria Catalysts[a]

sample	Au−O		Au−Au			
	R (Å)	CN	R (Å)	CN	σ^2 (Å^2)	ΔE_0 (eV)
Au_Atom (O_2, 300 °C)	1.96 ± 0.01	3.3 ± 0.3			0.004 ± 0.001	12.0 ± 1.3
Au_Cluster (WGS, 250 °C)	2.02 ± 0.03	0.8 ± 0.2	2.85 ± 0.04	0.9 ± 0.5	0.006 ± 0.002(O)	7.0 ± 1.9
					0.013 ± 0.006(Au)	
Au_Particle (O_2, 300 °C)			2.85 ± 0.01	10.0 ± 0.9	0.008 ± 0.001	5.6 ± 0.6
Au_Particle (WGS, 250 °C)			2.85 ± 0.01	11.5 ± 2.1	0.010 ± 0.002	5.2 ± 1.1

[a]R, distance; CN, coordination number.

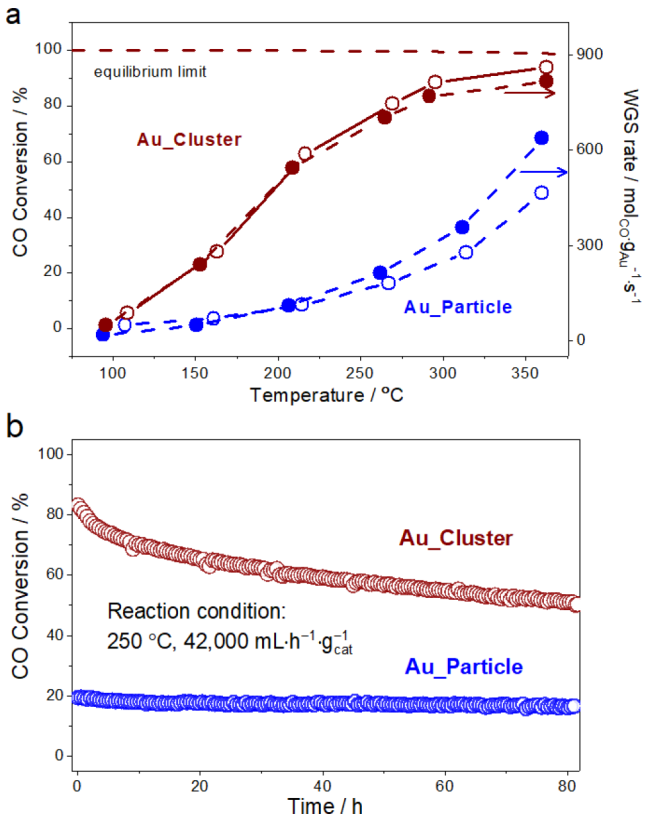

Figure 3. (a) Temperature-dependent CO conversion (hollow circles, left axis) and WGS reaction rate per molar Au (solid circles, right axis). The dotted line shows the thermodynamic equilibrium limit. (b) Long-term catalytic evaluation at 250 °C for Au_Cluster and Au_Particle. Reaction conditions: 2% CO/12% H_2O/N_2, GHSV = 42 000 mL·h^{-1}·g$_{cat}^{-1}$.

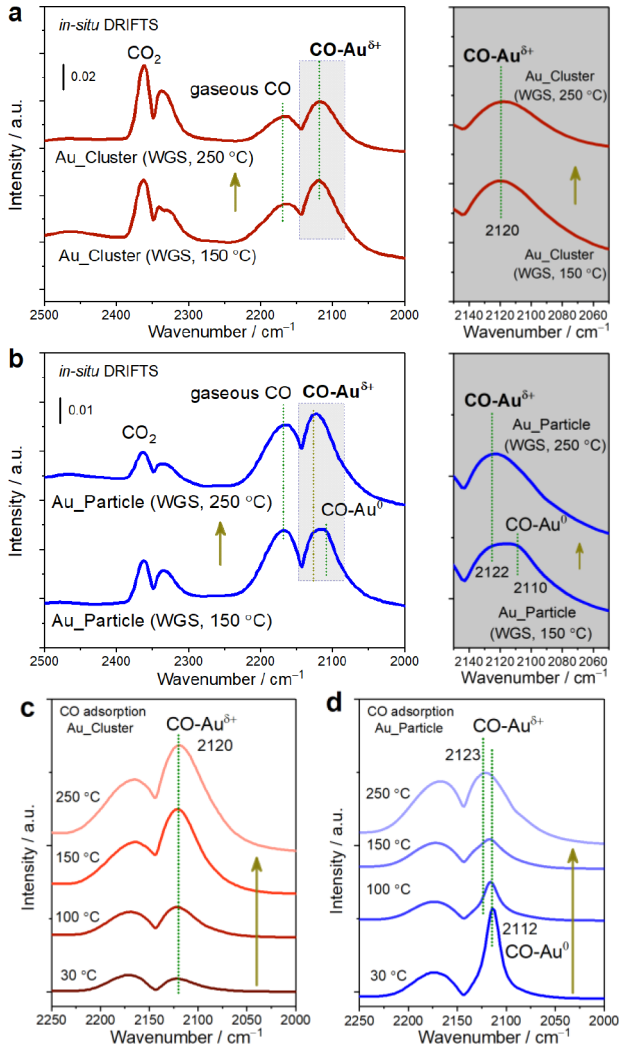

Figure 4. (a and b) In situ DRIFTS spectra of Au_Cluster and Au_Particle catalysts under WGS reaction conditions at T = 150 and 250 °C. Reaction condition: 2% CO/~3% H_2O/He, 30 mL/min, TOS = 1 h. Azure shadow illustrations are the enlarged area. (c and d) CO adsorption tests by in situ DRIFTS for Au_Cluster and Au_Particle at various temperatures. Reaction condition: 2% CO/He, 30 mL/min, TOS = 10 min.

for the large difference in activity for WGS between gold clusters and particles, we have done comprehensive in situ spectroscopic characterizations combining kinetics studies, which will be discussed in detail below.

Surface Site for CO Adsorption. Efficient CO adsorption, as the first step in catalyzing the WGS reaction, is curial to subsequent procedures on the catalyst surface. In situ DRIFTS measurements under WGS reaction conditions (2% CO/~3% H_2O/He, 150−250 °C) were conducted to detect the adsorbed CO species on the gold−ceria catalyst surface. For Au_Cluster, adsorbed CO on the unsaturated interface Au$^{\delta+}$[25] ($0 < \delta < 1$) sites at ~2120 cm^{-1} (CO-Au$^{\delta+}$, Figure 4a) was observed, coupling with the obvious CO_2 signal. For Au_Particle, at 150 °C, besides the interfacial CO-Au$^{\delta+}$ band, the CO-Au^0 band at ~2110 cm^{-1},[26−28] for which CO was adsorbed on these surface atoms of gold particles, was observed. At 250 °C, the CO-Au^0 band disappeared and only the CO-Au$^{\delta+}$ band was visible (Figure 4b).

To reveal the species evolution in CO adsorption, additional in situ DRIFTS measurements at different temperatures were further performed by using 2% CO/He as the adsorbent (Figure 4c,d). For the Au_Cluster catalyst, the initial status of the gold species was fully oxidized Au single atoms those are saturation coordinated with oxygen atoms, thus the adsorbed

DOI: 10.1021/jacs.8b09306
J. Am. Chem. Soc. 2019, 141, 4613−4623

signal was extremely weak and difficult to detect[25] in the initial stage at 30 °C (Figure 4c). Along with the temperature increasing, fully oxidized gold atoms were gradually reduced by CO, and some of the oxygen atoms that were coordinated with the gold atom were removed. Then these single gold atoms transformed into gold clusters coupled with the lower oxidation state of $Au^{\delta+}$ ($0 < \delta < 1$). Thus, the CO adsorption on interfacial gold atoms ($CO\text{-}Au^{\delta+}$) in a gold cluster gradually prevailed with increasing temperature.

For the Au_Particle catalyst, owing to the large size of Au nanoparticles, only a small population of interfacial atoms anchored to the matrix are positively charged, as schematically illustrated in Figure S6. Therefore, CO adsorption on the large number of surface gold atoms (~2113 cm^{-1}, $CO\text{-}Au^0$) in the gold nanoparticles dominated at a low temperature of 30 °C. The vibrational DRIFTS band corresponding to $CO\text{-}Au^0$ at around 2113 cm^{-1} promptly faded away with the increase in the adsorption temperature (Figure 4d) because of its low stability.[29,30] In contrast, the CO adsorption on interfacial gold sites (~2121 cm^{-1}) in Au_Particle became dominant. The evolution from $CO\text{-}Au^0$ to $CO\text{-}Au^{\delta+}$ was further proven for Au_Particle during consecutive ramping procedures (from 30 to 300 °C, 10 °C/min, Figure S7).

The above results revealed that, on one hand, the CO molecules that adsorbed on noninterfacial Au atoms in Au_Particle catalyst were hardly preserved under the WGS reaction condition (>150 °C). On the other hand, although CO adsorbed stably on the surface gold atoms in Au_Particle (Figure 4d) at relatively low temperatures of 100−150 °C, the WGS reaction rate on Au_Particle was only one-fifth to one-third of that on Au_Cluster (18−48 vs 49−240 $mol_{CO}\cdot g_{Au}^{-1}\cdot s^{-1}$). This fact implied that $CO\text{-}Au^0$ was intrinsically inactive for the WGS reaction. Interestingly, the superior CO adsorption on metallic Au_Particle was considered to be the induction of its excellent catalytic performance in CO oxidation at room temperature;[25] however, these surface Au atoms in gold particles were spectators in the WGS reaction.

The above results from CO adsorption measurements are well in line with the kinetics studies (Figure 5). The apparent reaction orders of CO for Au_Particle are 0.97 at 150 °C and 0.75 at 250 °C, respectively, implying insufficient CO adsorption in the WGS reaction. Au_Cluster showed obviously smaller n_{CO} values that are 0.51 at 150 °C and 0.59 at 250 °C, indicating advanced CO adsorption at the interfacial Au sites. On account of the distinctly different configurations of cluster and particle, various CO adsorption behaviors were performed on the differently polarized atoms of Au_Cluster and Au_Particle catalysts, thus inducing superior apparent activation energy (E_a) of Au_Cluster compared to that of Au_Particle (Figure S8) in the low-temperature range. So far, the identification of active Au sites in the WGS reaction is still under debate.[1,2,20,21,30,31,32] Here, we have precisely identified the inactive nature of the Au^0 species with Au−Au coordination in gold nanoparticles due to its inferior CO adsorption ability under the WGS reaction conditions. Only the $CO\text{-}Au^{\delta+}$ species that adsorbed on the gold atoms at the gold−ceria interfaces make real contributions to the reactivity.

Active Configuration of Surface Hydroxyls. After determining the active sites of adsorbed CO molecules, we then tried to identify the role of hydroxyl groups (−OH) dissociated from H_2O activation, which was regarded to be the rate-determining step for the WGS reaction.[14] By using the in situ DRIFTS technique, the band at ~3705 cm^{-1} observed

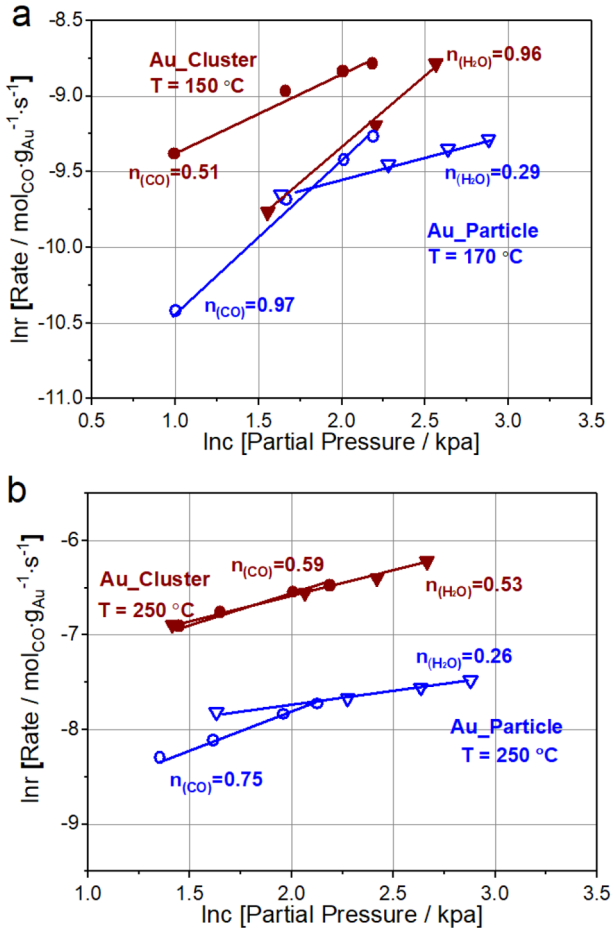

Figure 5. (a and b) Kinetic orders of the reactants (CO and H_2O) for Au_Cluster and Au_Particle at low (150 or 170 °C) and high temperatures (250 °C), respectively.

after introducing trace moisture at 150 °C (Figure 6a, left) is attributed to the terminal −OH singly bonded with the Ce^{4+} ion.[18,33,34] Another stretching band at ~3650 cm^{-1} is assigned to the bridged −OH groups.[33−35] These two types of −OH groups can be easily exchanged with isotopic H_2O (Figure S9a−c), thus their formation was strongly related to the dissociation of molecular H_2O.[24] When 2% CO/He feed was injected into these prehydroxylated samples, these two types of surface −OH groups were partially consumed (Figure 6a, right). Specifically, the elimination of terminal −OH groups at ~3705 cm^{-1} was detected for both Au_Cluster and Au_Particle catalysts at 150 °C. Thus, this terminal surface −OH group was much less irrelevant to the catalytic reactivity since Au_Particle had a very low reactivity of ~48 $mol_{CO}\cdot g_{Au}^{-1}\cdot s^{-1}$ at 150 °C (Figure 3a, right). Notably, bridged −OH groups centered at ~3653 cm^{-1} were abundantly consumed for Au_Cluster after the introduction of CO (Figure 6a), coupling with a much higher WGS activity of ~240 $mol_{CO}\cdot g_{Au}^{-1}\cdot s^{-1}$. As a sharp contrast, negligible changes in bridged −OH groups were observed for inactive Au_Particle. This distinct phenomenon was also confirmed from the similar evolution of bridged −OD groups at ~2690 cm^{-1} after CO injection (Figure 6b).

Subsequently, CO_2 was produced with the consumption of hydroxyls as shown in Figure S10a. To gain insight into the origin of the CO_2 product, the hydroxyls of both catalysts were already isotope-labeled (−$O^{18}H$, as seen in the Experimental

DOI: 10.1021/jacs.8b09306
J. Am. Chem. Soc. 2019, 141, 4613−4623

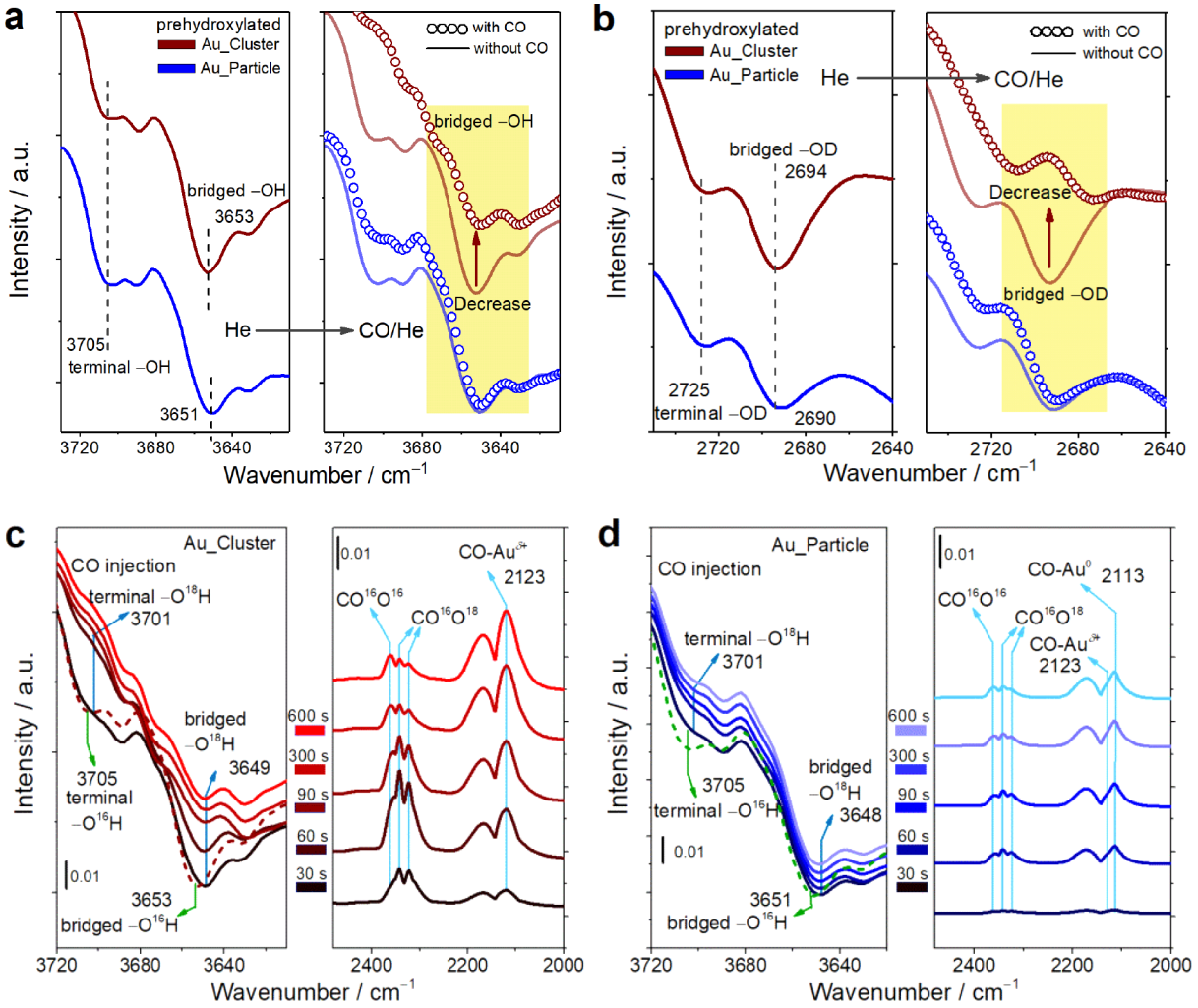

Figure 6. Determination of the role of bridged −OH groups in catalyzing the WGS reaction. (a) −OH region IR spectra of Au_Cluster and Au_Particle after prehydroxylation and then flow into CO at 150 °C (red, Au_Cluster; blue, Au_Particle from He to 2% CO/He, 30 mL/min, TOS = 1 h). The solid lines are the corresponding spectra before CO injections. For more accurate identification, the DRIFTS spectra of the −OH region are the raw data (negative peak). (b) −OD region IR spectra of Au_Cluster and Au_Particle after hydroxylation by D_2O and then flow into CO under the same conditions as in Figure 6a. Time-sequencing −OH region and C═O region IR spectra collected under CO injection for catalysts isotopically prelabeled by using H_2O^{18}: (c) Au_Cluster and (d) Au_Particle. The dashed lines are the reference spectra collected after prehydroxylation with H_2O^{16}.

Methods section). As expected, abundant $CO^{16}O^{18}$ products were generated for Au_Cluster once CO was injected (Figure 6c), directly proving that the −OH groups were involved in producing CO_2 exactly while an inferior amount of $CO^{16}O^{18}$ was generated for inactive Au_Particle as shown in Figure 6d. These results strongly proved a hydroxyl-involved reaction pathway for WGS catalyzed by the gold−ceria catalyst. It is noticed that, for both catalysts, the tricoordinated −OH groups at ∼3520 cm^{-1} were scarcely consumed after injecting CO molecules (Figure S10b), indicating the spectator role of this overcoordinated −OH group.

Temperature-programmed surface reaction (TPSR) tests were conducted on the prehydroxylated gold−ceria catalysts to further identify the roles of different types of −OH groups in the surface reaction. Generally, two stages were observed for the reaction between CO molecules and surface oxygenated species (Figure 7). In the low-reactivity α stage (30 to 150 °C) in the TPSR profile of both catalysts (Figure S11), the appearance temperatures of labeled COO^{18} (30−50 °C) were consistent with the consumption temperatures of terminal −OH at ∼3710 cm^{-1} as shown in Figure S12. Thus, the consumption of residually dry $[O]^2$ (Figure S13) and terminal −OH groups induced the initial CO_2 formation, which was less relevant to WGS reactivity. In the β stage, for Au_Cluster (Figure 7a), the coproduction of CO_2 and H_2 with a stoichiometric ratio of ∼2:1 started around 120 °C after CO introduction, which was in good agreement with the temperature range (100−150 °C) of the consumption of bridged −OH groups (Figure S12a). This proves that the surface reaction between bridged −OH groups and CO molecules exactly led to the formation of WGS products of CO_2 and H_2. Besides, as for Au_Particle, coproducts of CO_2 and H_2 appeared at the higher temperature of 220 °C (Figure 7b), which was also consistent with the fact that surface bridged −OH groups were consumed at 200−250 °C as shown in in situ DRIFTS measurements (Figure S12b). Additionally, as shown in Figure S14, no detectable H_2 signal (m/z = 2) could be observed for the prehydroxylated Au_Cluster catalyst during the He-TPD test. This evolution clearly revealed that surface −OH groups cannot further decompose to generate H_2

DOI: 10.1021/jacs.8b09306
J. Am. Chem. Soc. 2019, 141, 4613−4623

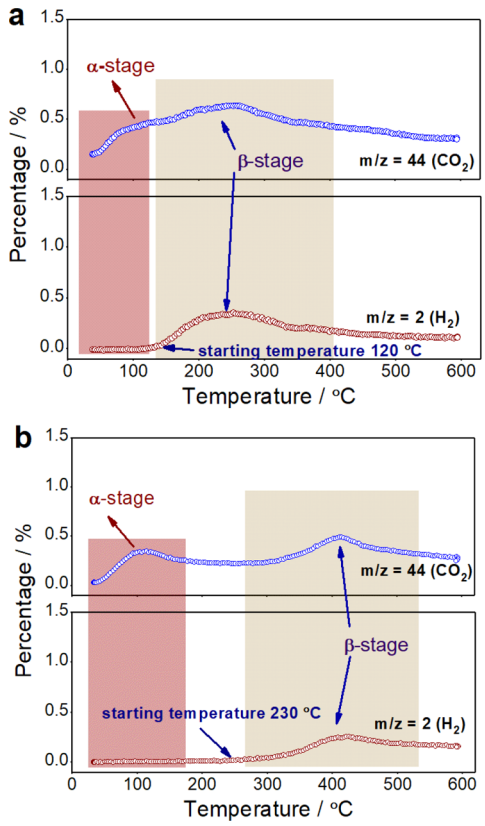

Figure 7. TPSR profiles for prehydroxylated (a) Au_Cluster and (b) Au_Particle. Signals of H_2 (m/z = 2) and CO_2 (m/z = 44) were detected. CO_2 and H_2 were coproduced in a stoichiometric ratio of ~2:1. The samples were pretreated with ~3% H_2O/He for 20 min at 200 °C and then purged with pure He at 200 °C to remove the adsorbed H_2O. Finally, the signal evolution was collected under 2% CO/He at a ramping rate of 5 °C/min for all of the above measurements.

(−OH → O* + H*, H* + H* → H_2) when the temperature was as high as 600 °C in the absence of CO molecules, proving that the primary reaction pathway in WGS over this gold−ceria catalyst consisted of CO molecules reacted with surface −OH groups following the associative pathways[6,11,14] rather than the redox pathway.[1,36]

Therefore, we concluded that the abundant interfacial sites in Au_Cluster effectively promoted the reaction between CO-$Au^{\delta+}$ and bridged −OH groups (CO + OH → CO_2 + $^1/_2H_2$), while the insufficient CO adsorption caused by limited interfacial gold sites drove the inferior ability to react with bridged −OH groups and correspondingly lower WGS activity for Au_Particle. Even though it has been reported that hydroxyl groups are involved in the WGS reaction,[2,19,37] direct proof of the exact active configuration is always lacking. Here, all of the above experimental results explicitly demonstrated that among all types of −OH groups on the gold−ceria catalyst surface, only the bridged one acts as the key active species in the WGS reaction.

Role of Surface Oxygen Vacancies. The role of oxygen vacancies on reducible supports in catalyzing the WGS reaction has been highlighted. It is reported that the dissociation of H_2O at oxygen vacancies is more thermodynamically preferred over a perfect CeO_2 surface.[38−40] Here, we carried out in situ Raman tests to explore the role of oxygen vacancies in water activation (Figure S15).[41] The vis-Raman spectra of CeO_2 are dominated by the strong F_{2g} mode of the fluorite phase at 451 cm^{-1} and the defect-induced mode (D) (surface defects at 560 cm^{-1} and intrinsic defects at 590 cm^{-1}).[42] The integral intensity ratio of D/F_{2g} that represents the relative concentration of oxygen vacancies was determined under three different atmospheres (CO/He, H_2O/He, and CO/H_2O/He). The statistical results of D/F_{2g} are shown in Figure 8a, and the Δ value (D/F_{2g}-CO/He − D/F_{2g}-H_2O/He) followed a sequence of Au_Cluster (0.19) > Au_Particle (0.14) > CeO_2 support (0.07), revealing the different abilities to consume surface oxygen vacancies under a H_2O feed. This also implied that the gold−ceria interface could enhance the water activation ability in the catalysts.[14] Furthermore, once the mixture of CO/H_2O was injected, distinct D/F_{2g} values were detected. For Au_Cluster, D/F_{2g} ≅ 0.30 under the WGS reaction condition was similar to that under the CO feed only, indicating the easy recovery of oxygen vacancies in the reaction. On the other hand, the full regeneration of surface oxygen vacancies under CO/H_2O also indicates that the WGS reaction rate was determined by the supply of active −OH species. Therefore, the H_2O dissociation step plays a more crucial role in gold cluster catalyst at low temperatures, which is well in line with the high apparent reaction order of H_2O

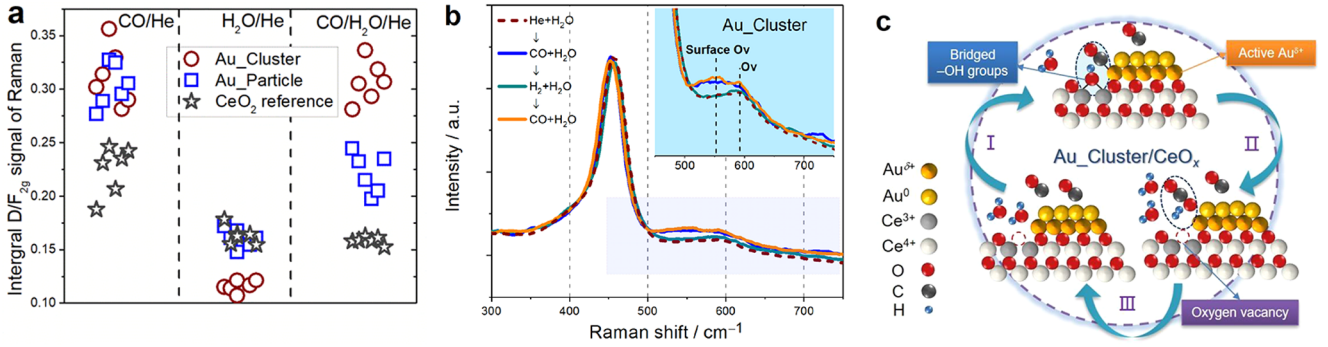

Figure 8. (a) Statistical results of the D/F_{2g} integral intensity ratio based on the in situ Raman results under different conditions as shown in Figure S15a. Raman spectra of Au_Cluster, Au_Particle, and the CeO_2 reference (CeO_2 nanorods) collected under various conditions (2% CO/He, ~3% H_2O/He, and 2% CO/~3% H_2O/He) at 150 °C. (b) In situ Raman spectra of Au_Cluster collected under various conditions at 150 °C: ~3% H_2O/He → 2% CO/~3% H_2O/He → 5% H_2/~3% H_2O/He → 2% CO/~3% H_2O/He. The shadowed area is the enlarged spectra. (c) Schematic illustration of the reaction mechanism on the interface of Au_Cluster catalysts: red, O; yellow, Au (dark yellow represents the interfical $Au^{\delta+}$); white, Ce^{4+}; gray, Ce^{3+}; blue, H; and black, C.

DOI: 10.1021/jacs.8b09306
J. Am. Chem. Soc. 2019, 141, 4613−4623

(n_{H_2O} = 0.96) for Au_Cluster at 150 °C. Considering that water dissociation is endothermic, the number of derived −OH groups on the catalyst surface increased with increasing temperature, thus the apparent kinetic reaction order of H_2O decreased correspondingly at 250 °C (n_{H_2O} = 0.53).

In contrast, Au_Particle exhibited an ability to generate surface oxygen vacancies in the WGS reaction, and the D/F_{2g} values were recovered only to ∼0.22 in the CO/H_2O feed versus that of ∼0.30 in the CO/He feed. This means that dissociated −OH groups are rich enough to react with the insufficiently adsorbed CO on the interfacial Au atoms for Au_Particle. As expected, a relatively small reaction order of H_2O for Au_Particle (n_{H_2O} = 0.29 at 170 °C), coupled with a high n_{CO} value of 0.95, implies the higher coverage[9] of residual −OH groups due to an insufficient supply of adsorbed CO. The distinct regeneration ability of surface oxygen vacancies for these catalysts was well matched with their WGS reaction rate, revealing that surface oxygen vacancies were indeed involved in catalyzing the surface reaction.

To further explore the relation between the formation of surface oxygen vacancies and the consumption of hydroxyls, we conducted additional in situ Raman measurements by switching various flows. As shown in Figure 8b, when the flowing gas mixture in the chamber changed from ∼3% H_2O/He to 2% CO/∼3% H_2O/He, the signal of surface oxygen vacancies at ∼560 cm^{-1} was obviously detected. However, such a phenomenon was not found after 5% H_2/∼3% H_2O/He feeding in. This special distinction confidently proved that these surface oxygen vacancies during the WGS reaction could be generated only through the reaction between bridged hydroxyls with CO, instead of that between surface dry $[O]$[2] atoms and H_2. Therefore, as schematically illustrated in Figure 8c, it is just the active bridged −OH groups generated from water dissociation rather than the other oxygen species including dry [O] and terminal hydroxyls (Figure S16) that occupied these renewable surface oxygen vacancies. Thus, following the reaction of adsorbed CO molecules with bridged −OH species, subsequent formation of a certain intermediate must take place on the metal−oxide interface.[5,6,19,43] Here, the formate (HCOO) configuration was prudently excluded as a dominant intermediate by purposely designed contrast experiments (Figures S17 and S18). The structural determination of the actual intermediate that decomposes to CO_2 and H_2 will be conducted in future work.

CONCLUSIONS

Our systematic investigations under various experimental conditions, especially with the aid of comprehensive in situ characterizations, confidently illustrated that the bridged surface hydroxyl is the sole reactive configuration among various hydroxyls in the surface of gold−ceria catalysts for the WGS reaction. These reactive bridged hydroxyls are derived from water dissociation on the surface oxygen vacancies of the nanoceria support. The surface reaction between bridged hydroxyls and CO molecules adsorbed on interfacial Au atoms contributes dominantly to the WGS reactivity. Therefore, the Au_Cluster catalyst with abundant interfacial sites performs much better than Au_Particle in catalyzing the WGS reaction. On account of this finding that can be obtained under different WGS reaction conditions, we reasonably believe that the conclusions drawn in this work were universal in the Au/CeO_2 system. The precise identification of bridged surface hydroxyl as key reactive species in this work greatly deepens the understandings of the reaction mechanism of the WGS reaction catalyzed by a supported gold catalyst at the atomic level.

ASSOCIATED CONTENT

Supporting Information

The Supporting Information is available free of charge on the ACS Publications website at DOI: 10.1021/jacs.8b09306.

Further experimental data, including XRD, XPS, in situ DRIFTS, in situ Raman, and TPSR results (PDF)

AUTHOR INFORMATION

Corresponding Authors

*jiacj@sdu.edu.cn
*sirui@sinap.ac.cn
*yan@pku.edu.cn

ORCID

Chao Ma: 0000-0001-8599-9340
Chun-Jiang Jia: 0000-0002-4254-5100
Chun-Hua Yan: 0000-0002-0581-2951

Notes

The authors declare no competing financial interest.

ACKNOWLEDGMENTS

Financial support was obtained from the Excellent Young Scientists Fund from the National Science Foundation of China (NSFC) (grant no. 21622106), other projects from the NSFC (grant nos. 21331001, 21773288, and 21771117), the Outstanding Scholar Fund (grant no. JQ201703), the Doctoral Fund (grant no. ZR2018BB010) of the Science Foundation of Shandong Province of China, the Taishan Scholar Project of Shandong Province of China, the Hundred Talents Project of the Chinese Academy of Sciences, and the Foundation of State Key Laboratory of Coal Conversion (grant no. J17-18-902). We thank Mr. Jun-Xiang Chen, Mr. Dao-Lei Wang, and Miss Lu Shen (Tilon GRP Technology Limited) for their kind help with the mass spectra measurements and data analysis. We thank the Center of Structural Characterization and Property Measurements at Shandong University for help with sample characterization.

REFERENCES

(1) Fu, Q.; Saltsburg, H.; Flytzani-Stephanopoulos, M. Active nonmetallic Au and Pt species on ceria-based water-gas shift catalysts. *Science* **2003**, *301*, 935−938.

(2) Yang, M.; Li, S.; Wang, Y.; Herron, J. A.; Xu, Y.; Allard, L. F.; Lee, S.; Huang, J.; Mavrikakis, M.; Flytzani-Stephanopoulos, M. Catalytically active Au-$O(OH)_x$- species stabilized by alkali ions on zeolites and mesoporous oxides. *Science* **2014**, *346*, 1498−1501.

(3) Rodriguez, J. A.; Ma, S.; Liu, P.; Hrbek, J.; Evans, J.; Pérez, M. Activity of CeO_x and TiO_x nanoparticles grown on Au(111) in the water-gas shift reaction. *Science* **2007**, *318*, 1757−1760.

(4) Song, W. Y.; Hensen, J. M. Mechanistic aspects of the water−gas shift reaction on isolated and clustered Au atoms on Ceo2(110): a density functional theory study. *ACS Catal.* **2014**, *4*, 1885−1892.

(5) Yao, S.; Zhang, X.; Zhou, W.; Gao, R.; Xu, W.; Ye, Y.; Lin, L.; Wen, X.; Liu, P.; Chen, B.; Crumlin, E.; Guo, J.; Zuo, Z.; Li, W.; Xie, J.; Lu, L.; Kiely, C. J.; Gu, L.; Shi, C.; Rodriguez, J. A.; Ma, D. Atomic-layered Au clusters on α-MoC as catalysts for the low-temperature water-gas shift reaction. *Science* **2017**, *357*, 389.

(6) Rodriguez, J. A.; Ramírez, P. J.; Asara, G. G.; Viñes, F.; Evans, J.; Liu, P.; Ricart, J. M.; Illas, F. Charge polarization at a Au-TiC

DOI: 10.1021/jacs.8b09306
J. Am. Chem. Soc. 2019, 141, 4613−4623

interface and the generation of highly active and selective catalysts for the low-temperature water-gas shift reaction. *Angew. Chem., Int. Ed.* **2014**, *53*, 11270−11274.
(7) Si, R.; Flytzani-Stephanopoulos, M. Shape and crystal-plane effects of nanoscale ceria on the activity of Au-CeO2 catalysts for the water-gas shift reaction. *Angew. Chem., Int. Ed.* **2008**, *47*, 2884−2887.
(8) Zhang, Z.; Wang, S.; Song, R.; Cao, T.; Luo, L.; Chen, X.; Gao, Y.; Lu, J.; Li, W.; Huang, W. The most active Cu facet for low-temperature water gas shift reaction. *Nat. Commun.* **2017**, *8*, 488.
(9) Shekhar, M.; Wang, J.; Lee, W.; Williams, W. D.; Kim, S. M.; Stach, E. A.; Miller, J. T.; Delgass, W. N.; Ribeiro, F. H. Size and support effects for the water−gas shift catalysis over gold nanoparticles supported on model Al_2O_3 and TiO_2. *J. Am. Chem. Soc.* **2012**, *134*, 4700−4708.
(10) Zhao, Z.; Li, Z.; Cui, Y.; Zhu, H.; Schneider, W. F.; Delgass, W. N.; Ribeiro, F.; Greeley, J. Importance of metal-oxide interfaces in heterogeneous catalysis: A combined DFT, microkinetic, and experimental study of water-gas shift on Au/MgO. *J. Catal.* **2017**, *345*, 157−169.
(11) Mudiyanselage, K.; Senanayake, S. D.; Feria, L.; Kundu, S.; Baber, A. E.; Graciani, J.; Vidal, A. B.; Agnoli, S.; Evans, J.; Chang, R.; Axnanda, S.; Liu, Z.; Sanz, J. F.; Liu, P.; Rodriguez, J. A.; Stacchiola, D. J. Importance of the metal-oxide interface in catalysis: in situ studies of the water-gas shift reaction by ambient-pressure x-ray photoelectron spectroscopy. *Angew. Chem., Int. Ed.* **2013**, *52*, 5101−5105.
(12) Yang, M.; Allard, L. F.; Flytzani-Stephanopoulos, M. Atomically dispersed Au−$(OH)_x$ species bound on titania catalyze the low-temperature water-gas shift reaction. *J. Am. Chem. Soc.* **2013**, *135*, 3768−3771.
(13) Ta, N.; Liu, J.; Chenna, S.; Crozier, P. A.; Li, Y.; Chen, A.; Shen, W. Stabilized gold nanoparticles on ceria nanorods by strong interfacial anchoring. *J. Am. Chem. Soc.* **2012**, *134*, 20585−20588.
(14) Gokhale, A. A.; Dumesic, J. A.; Mavrikakis, M. On the mechanism of low-temperature water gas shift reaction on copper. *J. Am. Chem. Soc.* **2008**, *130*, 1402−1414.
(15) Shido, T.; Iwasawa, Y. Regulation of reaction intermediate by reactant in the water-gas shift reaction on CeO2, in relation to reactant-promoted mechanism. *J. Catal.* **1992**, *136*, 493−503.
(16) Cui, Y.; Li, Z.; Zhao, Z.; Cybulskis, V. J.; Sabnis, K. D.; Han, C. W.; Ortalan, V.; Schneider, W. F. Participation of interfacial hydroxyl groups in the water-gas shift reaction over Au/MgO catalysts. *Catal. Sci. Technol.* **2017**, *7*, 5257.
(17) Fishtik, I.; Datta, R. A UBI−QEP microkinetic model for the water−gas shift reaction on Cu(111). *Surf. Sci.* **2002**, *512*, 229.
(18) Badri, A.; Binet, C.; Lavalley, J.-C. An FTIR study of surface ceria hydroxy groups during a redox process with H_2. *J. Chem. Soc., Faraday Trans.* **1996**, *92*, 4669−4673.
(19) Leppelt, R.; Schumacher, B.; Plzak, V.; Kinnea, M.; Behm, R. J. Kinetics and mechanism of the low-temperature water−gas shift reaction on Au/CeO2 catalysts in an idealized reaction atmosphere. *J. Catal.* **2006**, *244*, 137−152.
(20) Kim, C. H.; Thompson, L. T. On the importance of nanocrystalline gold for Au/CeO_2 water−gas shift catalysts. *J. Catal.* **2006**, *244*, 248−250.
(21) Abdel-Mageed, A. M.; Kučerová, G.; Bansmann, J.; Behm, R. J. Active Au Species During the low-temperature water gas shift reaction on Au/CeO_2: A time-resolved operando XAS and DRIFTS study. *ACS Catal.* **2017**, *7*, 6471−6484.
(22) Mai, H. X.; Sun, L.-D.; Zhang, Y.-W.; Si, R.; Feng, W.; Zhang, H.-P.; Liu, H.-C.; Yan, C.-H. Shape-selective synthesis and oxygen storage behavior of ceria nanopolyhedra, nanorods, and nanocubes. *J. Phys. Chem. B* **2005**, *109*, 24380−24385.
(23) Comotti, M.; Li, W. C.; Spliethoff, B.; Schüth, F. Support effect in high activity gold catalysts for CO oxidation. *J. Am. Chem. Soc.* **2006**, *128*, 917−924.
(24) Vayssilov, G. N.; Mihaylov, M. P.; Petkov, S.; Hadjiivanov, K. I.; Neyman, K. M. Reassignment of the vibrational spectra of carbonates, formates, and related surface species on ceria: a combined density functional and infrared spectroscopy investigation. *J. Phys. Chem. C* **2011**, *115*, 23435−23454.
(25) Guo, L.; Du, P.; Fu, X.; Ma, C.; Zeng, J.; Si, R.; Huang, Y.; Jia, C.; Zhang, Y.; Yan, C. Contributions of distinct gold species to catalytic reactivity for carbon monoxide oxidation. *Nat. Commun.* **2016**, *7*, 13481.
(26) Green, I. X.; Tang, W.; McEntee, M.; Neurock, M.; Yates, J. T. Inhibition at perimeter sites of Au/TiO_2 oxidation catalyst by reactant oxygen. *J. Am. Chem. Soc.* **2012**, *134*, 12717−12723.
(27) Carrasquillo-Flores, R.; Ro, I.; Kumbhalkar, M. D.; Burt, S.; Carrero, C. A.; Alba-Rubio, A. C.; Miller, J. T.; Hermans, I.; Huber, G. W.; Dumesic, J. A. Reverse water−gas shift on interfacial sites formed by deposition of oxidized molybdenum moieties onto gold nanoparticles. *J. Am. Chem. Soc.* **2015**, *137*, 10317−10325.
(28) Chen, S. L.; Luo, L. F.; Jiang, Z. Q.; Huang, W. X. Size-dependent reaction pathways of low-temperature CO oxidation on Au/CeO_2 catalysts. *ACS Catal.* **2015**, *5*, 1653−1662.
(29) Lemire, C.; Meyer, R.; Shaikhutdinov, S. K.; Freund, H. J. CO adsorption on oxide supported gold: from small clusters to monolayer islands and three-dimensional nanoparticles. *Surf. Sci.* **2004**, *552*, 27−34.
(30) Mihaylov, M.; Knözinger, H.; Hadjiivanov, K.; Gates, B. C. Characterization of the oxidation states of supported gold species by IR spectroscopy of adsorbed CO. *Chem. Ing. Tech.* **2007**, *79*, 795−806.
(31) Deng, W.; Carpenter, C.; Yi, N.; Flytzani-Stephanopoulos, M. Comparison of the activity of Au/CeO_2 and Au/Fe_2O_3 catalysts for the CO oxidation and the water-gas shift reactions. *Top. Catal.* **2007**, *44*, 199−208.
(32) Ratnasamy, C.; Wagner, J. P. Water Gas Shift Catalysis. *Catal. Rev.: Sci. Eng.* **2009**, *51*, 325−440.
(33) Laachir, A.; Perrichon, V.; Badri, A.; Lamotte, J.; Catherine, E.; Lavalley, J. C.; Fallah, J.; Hilaire, E. L.; Normand, F. l.; Quemere, E.; Sauvion, G. N.; Touret, O. Reduction of CeO_2 by hydrogen. Magnetic susceptibility and Fourier-transform infrared, ultraviolet and X-ray photoelectron spectroscopy measurements. *J. Chem. Soc., Faraday Trans.* **1991**, *87*, 1601−1609.
(34) Badri, A.; Binet, C.; Lavalley, J. C. An FTIR study of surface ceria hydroxy groups during a redox process with H_2. *J. Chem. Soc., Faraday Trans.* **1996**, *92*, 4669−4673.
(35) Binet, C.; Daturi, M.; Lavalley, J. C. IR study of polycrystalline ceria properties in oxidised and reduced states. *Catal. Today* **1999**, *50*, 207−225.
(36) Nakamura, J.; Cambell, J. M.; Campbell, C. T. Kinetics and mechanism of the water-gas shift reaction catalysed by the clean and Cs-promoted Cu(110) surface: a comparison with Cu(111). *J. Chem. Soc., Faraday Trans.* **1990**, *86*, 2725.
(37) Ashok, J.; Ang, M. L.; Terence, P. Z. L.; Kawi, S. Promotion of the water-gas-shift reaction by nickel hydroxyl species in partially reduced nickel-containing phyllosilicate catalysts. *ChemCatChem* **2016**, *8*, 1308−1318.
(38) Ang, M. L.; Oemar, U.; Saw, E. T.; Mo, L.; Kathiraser, Y.; Chia, B. H.; Kawi, S. Highly active Ni/$_x$Na/CeO_2 catalyst for the water−gas shift reaction: effect of sodium on methane suppression. *ACS Catal.* **2014**, *4*, 3237−3248.
(39) Watkins, M. B.; Foster, A. S.; Shluger, A. L. Hydrogen cycle on CeO2 (111) surfaces: density functional theory calculations. *J. Phys. Chem. C* **2007**, *111*, 15337−15341.
(40) Vecchietti, J.; Bonivardi, A.; Xu, W.; Stacchiola, D.; Delgado, J. J.; Calatayud, M.; Collins, S. E. Understanding the role of oxygen vacancies in the water gas shift reaction on ceria-supported platinum catalysts. *ACS Catal.* **2014**, *4*, 2088−2096.
(41) Wu, Z.; Li, M.; Howe, J.; Meyer, H. M.; Overbury, S. H. Probing defect sites on CeO_2 nanocrystals with well-defined surface planes by Raman spectroscopy and O_2 adsorption. *Langmuir* **2010**, *26*, 16595−16606.
(42) Vindigni, F.; Manzoli, M.; Damin, A.; Tabakova, T.; Zecchina, A. Surface and inner defects in Au/CeO_2 WGS catalysts: relation

DOI: 10.1021/jacs.8b09306
J. Am. Chem. Soc. 2019, 141, 4613−4623

between Raman properties, reactivity and morphology. *Chem. - Eur. J.* **2011**, *17*, 4356−4361.
(43) Saw, E. T.; Oemar, U.; Tan, X. R.; Du, Y.; Borgna, A.; Hidajat, K.; Kawi, S. Bimetallic Ni−Cu catalyst supported on CeO_2 for high-temperature water−gas shift reaction: Methane suppression via enhanced CO adsorption. *J. Catal.* **2014**, *314*, 32−46.

DOI: 10.1021/jacs.8b09306
J. Am. Chem. Soc. 2019, 141, 4613−4623